Molecular Cross-Linking Enhances Stability of Non-Fullerene Acceptor Organic Photovoltaics

Sangcheol Yoon[1], Braulio Reyes-Suárez[2], Sang T. Pham[3], Hervé Vezin[4], Yeny A. Tobon[4], Myeongjae Lee[5], Sam Mugiraneza[1], Brian Minki Kim[1], Mariane Yuka Tsubaki Oide[1,6], Seongju Yoo[5], Seunggu Lee,[7] Shu Hui Wang[5], Sean M. Collins[3,8], Christopher M. Bates,[9] Yongsup Park,[7] BongSoo Kim[5,], G. N. Manjunatha Reddy[2,]*, Thuc-Quyen Nguyen[1,]**

[1]Center for Polymers and Organic Solids, Department of Chemistry and Biochemistry, University of California, Santa Barbara (UCSB), California 93106, United States

[2]University of Lille, CNRS, Centrale Lille Institut, Université d' Artois, UMR 8181, Unité de Catalyse et Chimie du Solide, Lille F-59000, France

[3]Bragg Centre for Materials Research & School of Chemical and Process Engineering, University of Leeds, Woodhouse Lane, Leeds LS2 9JT, UK

[4]University of Lille, CNRS UMR 8516 – LASIRE – Laboratoire de Spectroscopie pour les Interactions la Réactivité et l'Environnement Lille 59000, France

[5]Department of Chemistry, Ulsan National Institute of Science and Technology (UNIST), Ulsan 44919, Republic of Korea

[6]Department of Metallurgical and Materials Engineering, University of São Paulo, São Paulo 05508-030, Brazil

[7]Department of Physics, Department of Information Display, Research Institute of Basic Sciences, Kyung Hee University, Seoul 02447, Republic of Korea

[8]School of Chemistry, University of Leeds, Woodhouse Lane, Leeds LS2 9JT, UK

[9]Department of Materials, Department of Chemistry and Biochemistry, Department of Chemical Engineering, University of California, Santa Barbara (UCSB), California 93106, United States

Correspondence should be addressed to
quyen@chem.ucsb.edu, gnm.reddy@univ-lille.fr, bongsoo@unist.ac.kr

ABSTRACT

Understanding efficiency-durability relationships and related mitigation strategies is an important step towards commercialization of organic photovoltaics (OPVs). Here, we report that a photoactivated 6-bridged azide cross-linker (6Bx) improves the morphological stability by suppressing thermally activated diffusion of (Y6) acceptor molecules in PM6:Y6 bulk-heterojunction (BHJ)-based OPVs. Cross-linked PM6:Y6(0.05 wt% 6Bx) BHJ OPVs retain 93.4% of initial power conversion efficiency upon thermal aging at 85 °C for 1680 h (T_{80} = 3290 h). Molecular origins of enhanced thermal stability are corroborated by optical spectroscopy, surface imaging, 2D solid-state nuclear magnetic resonance (NMR), Raman spectroscopy and scanning electron diffraction (SED) measurements and analysis of the BHJ thin films. A facile single-step cross-linking strategy in conjugation with advanced characterization methods presented in the study paves the way towards developing durable OPVs based on non-fullerene acceptors (NFAs).

Table of Contents

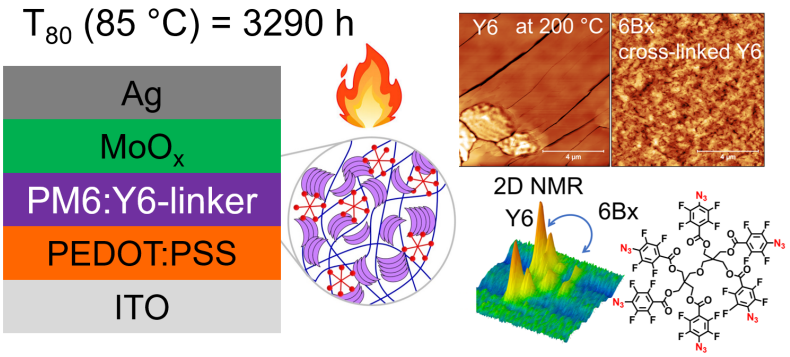

There is an upsurge in the solar-to-electrical power conversion efficiency (PCE) of BHJ based organic photovoltaic devices (OPVs) – thanks to the introduction of Y6 nonfullerene acceptor (NFA) combined with the PM6 polymer donor[1] – inviting further research in this field. Significant

efforts have been made in the development new NFAs[2-7] in order to boost PCEs to over 19%.[8-11] While these advancements represent an important leap forward towards commercialization of OPVs, there is an urgent need to address the device stability issues associated with these devices. The instability issues can be related to undesirable reactions at interfaces between the stacked layers in a device,[12-17] and more significantly in the photoactive layer caused either by thermal or photochemical processes.[18-28] It has been shown that the thermally induced molecular diffusion of NFAs significantly alters BHJ morphology leading to OPV performance deterioration.[19-21] For example, OPVs in outdoor settings are expected to operate under intense solar illumination at elevated operating temperatures,[29, 30] and can reach ~65 °C. Recently, two different mitigation strategies have been suggested to address thermally-induced instability issue in OPVs: synthesizing thermally robust materials (*e.g.* oligomers[31-35] or side group engineering in NFAs[36-38]), and cross-linking of donor (D) and acceptor (A) moieties in the BHJ morphology.[39] However, synthesizing thermally stable D and A materials requires expensive and rigorous synthesis procedures. Instead, cross-linking donor and/or acceptor can be viewed as a credible and sustainable approach that can be achieved by: (i) incorporating cross-linking units onto D or A during their synthesis, or (ii) adding them to D:A BHJ blends during solution casting process.

Inspired by the cross-linking methods that have been previously applied to suppress thermally induced aggregation of fullerenes (FAs) in OPV devices,[40-46] this approach has been extended to nascent all-polymer and NFA-based OPVs. For example, covalently cross-linked moieties on the D polymer side chains,[47, 48] polymeric acceptors or NFAs,[49, 50, 51] have been shown to improve stability in OPVs and other optoelectronic devices.[39] Noteworthy examples also include the addition of azide-based cross-linker additives added to the PM6 polymer layer to prepare a bilayer film consisting of PM6+cross-linker/Y6,[52, 53] to enhance photo- and thermal stability. In contrast,

studies have also reported the detrimental effects of single or double cross-linkable azide and diazirine moieties on the PM6:Y6 based OPVs,[54] by means of degradation products formed upon cross-linking of Y6 molecules leading to exciton quenching and performance deterioration. Despite the advancements in cross linking chemistry of NFAs, there remain several unaddressed questions regarding NFA stability in OPVs including thermally activated diffusion or aggregation of NFAs, enjoining further investigation. Here, we present a photoactivated cross linking approach using 6-bridged azide cross-linker (6Bx) to stabilize PM6:Y6 BHJ morphology to substantially improve the thermal stability of OPV devices. In so doing, we applied multimodal characterization techniques to unravel the BHJ morphological features and local structures that contribute to the enhanced OPV stability.

Figure 1a presents the chemical structures of PM6, Y6, and a molecular tether (6Bx) that is composed of 6 azide cross-linkable units. The 6Bx enables higher cross-linking efficiency (96%) compared to those with four (4Bx, 82%) and two azide units (2Bx, 36%).[55] Azide cross-linking can be triggered by either thermally activated or photoactivated methods using ultra-violet (UV) light irradiation.[56] Here, photoactivation (254 nm UV light) was used in order to avoid additional thermally-induced morphological degradation. UV light irradiation activates the azide moieties to generate a reactive singlet nitrene which reacts with alkyl chains by inserting into carbon-hydrogen bonds of the alkyl chains.[57-59] **Figure 1b** shows the energy levels of Y6, PM6, Y6:6Bx, PM6:6Bx obtained from the ultraviolet electron spectroscopy (UPS) and inverse photoelectron spectroscopy (IPES). Importantly, cross-linking of Y6 and PM6 with 0.05wt% of 6Bx does not significantly alter their energy levels.

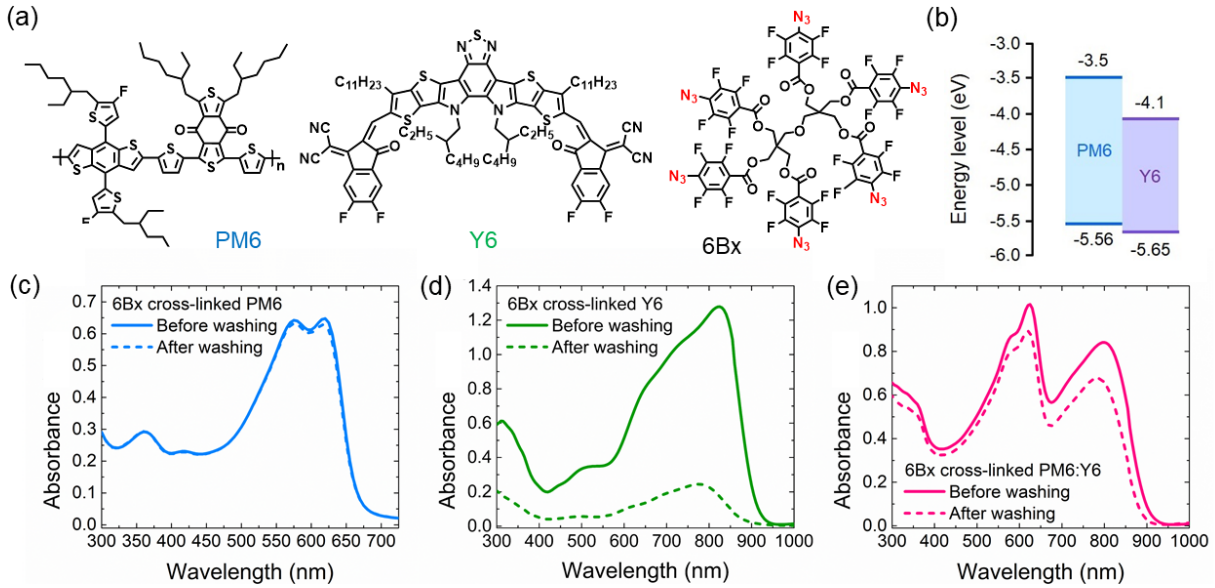

Figure 1. (a) Chemical structures of PM6, Y6, and 6Bx cross-linker. (b) Energy diagram of pristine and 0.05 wt% 6Bx cross-linked PM6 and Y6. Absorbance of 20 wt% 6Bx cross-linked (c) PM6, (d) Y6, and (e) PM6:Y6 BHJ films before and after washing with chloroform.

To confirm the photoactivation of azide units in 6Bx, we carried out Fourier-transform infrared (FTIR) spectroscopy measurements (**Figure S1**) in which the azide vibration at ~2125 cm^{-1} disappears after the UV light irradiation for 1 minute under nitrogen environment that activates azide cross-linking reactions.[60-62] A simple but credible method to confirm this trend is the use of a solubility test that involves washing of the 6BX treated materials using a solvent in which these material dissolve.[53, 63] Here, chloroform (CF) was used as washing solvent. Optical absorption spectra acquired before and after washing the 20 wt% 6Bx treated PM6 films with CF (**Figure 1c**) do not show significant changes in the absorbance, suggesting that the PM6 polymers (molecular weight, M_W = 77 kDa) are cross-linked by the 6Bx. On the other hand, the 20wt% of 6Bx treated Y6 acceptor molecules (M_W = 1.4 kDa) are severely affected by the washing process, resulting in the absorption loss (**Figure 1d**). Intriguingly, 20 wt% 6Bx cross-linked PM6:Y6 BHJ films

(**Figure 1e**) are much more robust toward this washing test, akin to PM6 films. In the PM6:Y6 morphology, cross-linked Y6 domains are much more likely to be retained during the washing process. In explaining this, we reasoned that the cross-linking of PM6 forms much larger networks compared to Y6. For example, a 6Bx moiety connecting two PM6 chains can double the molecular weight from 77 to 154 kDa, whereas cross-linking two Y6 molecules yields 2.8 kDa, as constrained by its size. Thus, achieving high crosslinking densities with Y6 requires a large amount of cross-linker, potentially impacting desired optoelectronic properties and OPV device efficiency (*vide infra*). Thus, *a priori*, we focused on exploring how the 6Bx cross-linking influences the morphological and thermal properties of Y6 films.

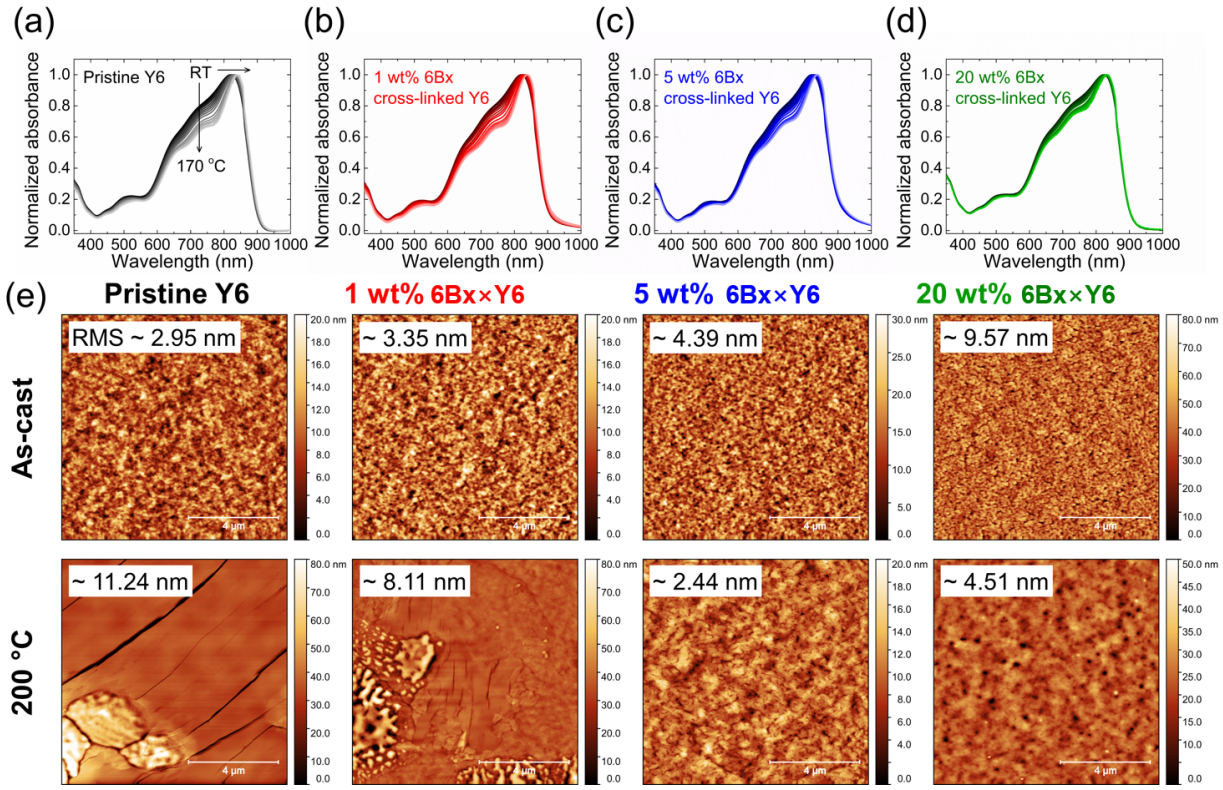

Figure 2. Normalized absorbance of (a) the pristine Y6 and the 6Bx cross-linked Y6 ((b) 1, (c) 5, and (d) 20 wt%) thin films annealed at increased temperatures from 40 to 170 °C. (e) AFM images (scan area: 10 × 10 μm^2) of the pristine Y6 and the 6Bx cross-linked Y6 (1, 5, and 20 wt%) thin films: as-cast films in an upper panel and the films annealed at up to 200 °C in a bottom panel.

Thermal stability is assessed by examining more closely the Y6 and the 6Bx cross-linked Y6 films (1, 5, and 20 wt% 6Bx) based on temperature dependent optical absorption and glass-transition temperature (T_g). The normalized absorbance spectra obtained upon thermal annealing at 40 – 170 °C range (10 °C intervals, each for 10 minutes) are compared (**Figure 2a-d)**, and the associated absorbance spectra are displayed in **Figure S2** and **Figure S3**. For the Y6 film, thermal annealing causes a red shift in the absorption (**Figure 2a**) due to molecular aggregation,[64-66] but the 6Bx cross-linked Y6 film shows more mitigated absorption shift at higher 6Bx (**Figure 2b**, **2c**, and **2d**). For the non-activated Y6:6Bx (*i.e.*, without UV photoactivation), on the other hand, the degree of the absorption red shift (**Figure S4**) is similar to that of Y6, because 6Bx does not cross-link Y6 molecules and these are able to aggregate like pristine Y6. These results indicate that the thermal diffusion and molecular aggregation of Y6 is restricted upon cross-linking with 6Bx. The results can be further verified by studying the glass-transition temperature (T_g), in which the cross-linking is expected to increase the T_g of materials.[67-69] For small molecule NFAs, however, it becomes less straight forward to measure the T_g values using differential scanning calorimetry (DSC).[21] Instead, UV–vis spectroscopy[70] has been used as an alternative to estimate the T_g of the NFAs,[20, 21, 31, 33, 34, 71] which is preferred in this study. The detailed description of this technique and deviation metric (DM_T) values are described in the SI. **Table 1** summarizes the estimated T_g value of Y6 and 6Bx cross-linked Y6 films. Upon cross-linking with 6Bx, the T_g value of the Y6 films slightly increases

Table 1. T_g of the pristine Y6 and the 6Bx cross-linked Y6 films (1, 5, and 20 wt%) estimated from the UV–vis absorption spectroscopy technique.

6Bx concentration (wt%)	T_g (°C)
0	91.9
1	92.3
5	96.9
20	97.9

from 91.9 °C (pristine Y6) to 92.3, 96.9, and 97.9 °C for 1, 5, and 20 wt% 6Bx, respectively. Their DM_T plots are presented in **Figure S5**. It is noteworthy that, for the non-activated Y6:6Bx, the DM_T plots (**Figure S6**) show that the thermal activation of 6Bx cross-linking occurs above 120 °C. Below 120 °C, their DM_T values are identical to that of pristine Y6 regardless of the 6Bx concentration (**Figure S6b**). The azide moieties of 6Bx start to activate at temperatures above 120 °C as detected in thermogravimetric analysis (TGA) of neat 6Bx (**Figure S7**). UV–vis spectroscopy results corroborate that 6Bx cross-linking restricts molecular aggregation of Y6 NFAs in the solid state and contributes to an increased T_g.

Subsequently, we analyzed the surface morphological features of the pristine Y6 and the 6Bx cross-linked Y6 films (1, 5, and 20 wt% 6Bx) using atomic force microscopy (AFM) and optical microscopy (OM) techniques. The AFM images were collected in both 2 × 2 and 10 × 10 μm^2 scan area (**Figures S8** and **S9)** as function of increasing temperature (80, 120, 150, 170, 180, and 200 °C, each for 10 min). As shown in **Figure 2e**, the root mean square (RMS) roughness of the pristine Y6 film is ~2.95 nm differs from the RMS values of cross-linked Y6 films ~3.35, 4.39, and 9.57 nm for 1, 5, and 20 wt% 6Bx, respectively. For Y6 film, thermal annealing at 200 °C causes significant molecular movement leading to large crystalline domains with a crack depth of ~50 nm, which is consistent with previous reports.[72, 73] It is noteworthy that the crystallization temperature of Y6 depends on film thickness: 20 and 60 nm-thick film exhibited crystallization-induced cracks at 180 °C (**Figure S10**) and at 200 °C, respectively. In contrast to this, 5 and 20 wt% 6Bx cross-linked Y6 films did not produce such features on their surfaces, confirming that 6Bx cross-linking helps preventing Y6 molecules from being crystallized at high temperatures. At relatively larger length scales of several tens of microns, OM analysis of the pristine Y6 and the 20 wt% 6Bx cross-linked Y6 films (**Figure S11**, acquired before and after the annealing at 200 °C) provided

additional support for such morphological evolution: the crystal growth of Y6 molecules is evident in the pristine Y6 film only, and is not observed in the 6Bx cross-linked Y6 film. Furthermore, OM analysis of pristine PM6:Y6 BHJ and 5 wt% 6Bx cross-linked PM6:Y6 BHJ films upon annealing at a harsh condition (200 °C for 1 h, see **Figure S12**) shows that the 6Bx cross-linked BHJ morphology is relatively resistant to thermal stress, but the pristine BHJ morphology displays dramatic changes on the surface. Together, these results and analyses indicates 6Bx cross-linking effectively suppresses molecular aggregation and crystallization of Y6 in the solid state.

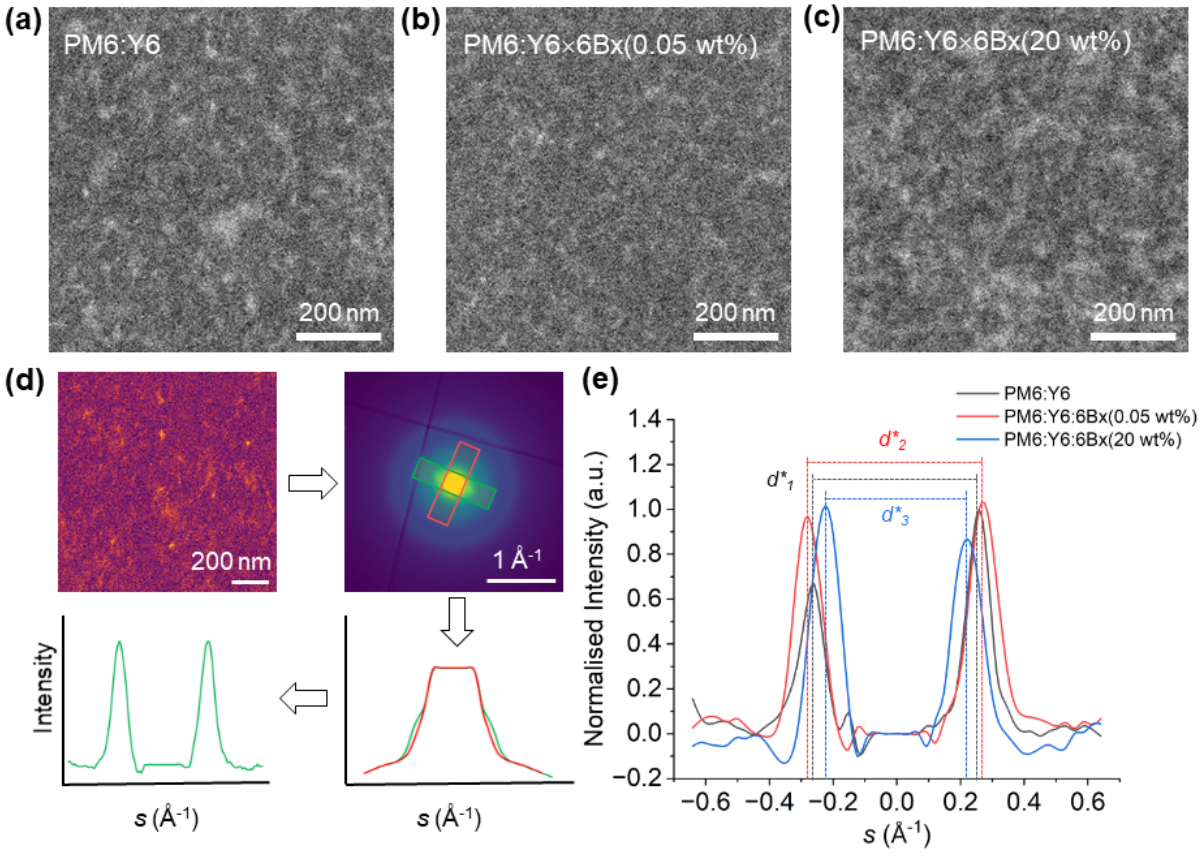

Figure 3. Scanning Electron Diffraction analysis of PM6:Y6 and PM6:Y6 cross-linked by 6Bx. (a-c) Annular dark field (ADF) images of PM6:Y6, PM6:Y6:6Bx (0.05 wt%), and PM6:Y6:6Bx (20 wt%), respectively, showing systematic changes in the morphology of diffracting domains with the addition of 6Bx. (d) Illustration of the analysis procedure for extracting the position of the Friedel pairs (diffraction vectors $\mathbf{g}_{400}$ and $\mathbf{g}_{\bar{4}00}$: more details are presented in SI) used to determine $d_{\pi-\pi}$ from the electron diffraction data. (e) Plot of Friedel pairs position in the

diffraction pattern showing a shift after crossing-linking with 6Bx. With 20wt% 6Bx, a decrease in reciprocal space distance d* (peak-to-peak distance) corresponding to an increase in *d*-spacing ($2/d^*_{peak\text{-}to\text{-}peak}$) is observed.

Although the above results indicate that the cross-linked Y6 molecules exhibit enhanced thermal stability in thin films, it is unclear that the molecular origins that contribute to the enhanced stability in PM6:Y6 BHJ thin films and the associated OPV devices. To resolve the morphology of pristine and cross linked PM6:Y6 BHJ films, we applied the scanning electron diffraction (SED) technique, a low-dose variant of four-dimensional scanning transmission electron microscopy (4D-STEM) established as a method for unravelling the nanoscale ordering and domain structure in organic semiconductor films and particularly their π-π interplanar spacings and the relative orientation of π-π stacking planes.[74, 75] In SED, a two-dimensional diffraction pattern is acquired at every position (pixel) in an image acquired by scanning an electron 'pencil beam' (focused probe with small convergence angle) across a thin sample. First, a diffraction-contrast annular dark field (ADF) STEM images was formed, revealing an interwoven BHJ morphology (**Figure 3a-c**). The brighter features in these images were traced to weak but detectable Bragg diffraction spots, characteristic features of crystalline domains. These crystalline domains are expected to originate from the Y6 acceptor regions that are relatively more crystalline compared to the PM6 donor polymer. A step-by-step protocol to analyze these images is presented in **Figure 3d** (and SI, experimental**)**: first, the circular virtual aperture (circular mask on the diffraction axes) is kept at the approximate scattering angle for $d_{\pi-\pi}$ to produce a virtual dark field (VDF) image in the vicinity of the scattering angle characteristic for π–π stacking, showing a localised domain. Then, a threshold intensity is defined to detect the regions in the real-space VDF image with strong scattering intensity. A diffraction pattern is then formed by averaging the diffraction patterns from all probe positions with intensity above the threshold (filtered patterns with high relative scattering

intensity at the characteristic angular range for $d_{\pi-\pi}$). Two intensity profiles can then be extracted, one spanning the scattered Friedel pair profile (marked by a green rectangular) and a second profile at a perpendicular orientation (unstructured scattering, marked by a red rectangular) observed as subtracted background from the profile spanning the Bragg reflections. The diffraction spots (**Figure 3d**) can be indexed to the {400} reflections for the Y6 unit cell, i.e., the π–π stacking distance $d_{\pi-\pi}$ between Y6 molecules. However, these crystalline domains do not appear to show any long-range coherent in-plane orientation, as evidenced by varied orientations of the Friedel pairs observed at approximately the π–π distance ({400} reflections) for the Y6 unit cell observed in different nano-crystalline domains across the film (**SI, Figures S13-S15**). For PM6:Y6 and PM6:Y6:6Bx (0.05wt%), the average of coherent scattering domains (i.e. crystallites with a single orientation) is <30 nm in size (SI, **Figures S13-S15**), consistently with Resonant Soft X-ray Scattering (RSoXS) data analysis presented for the PM6:Y6 BHJ morphology.[76] It suggests that the addition of +0.05wt%, does not substantially modify the BHJ morphology. In contrast to this, the diffracting domains in PM6:Y6:6Bx (20wt%) (**Figures 3c, S15**) appear to show an increased spread of sizes. The π–π stacking distance, extracted as twice the inverse of the Bragg (reciprocal space, $Å^{-1}$) peak-to-peak distance $2/d^*_{\text{peak-to-peak}}$ (we adopt the electron diffraction convention, such that $d^*_{\text{peak-to-peak}}/2 = 1/d_{\pi-\pi}$) shows a corresponding similarity for PM6:Y6 and PM6:Y6+0.05wt% at 3.87 ± 0.06 Å and 3.71 ± 0.09 Å, respectively. The π–π stacking distance in neat Y6 films is reported to centre at 3.57-3.59 Å, and the distribution centre increases to 3.61-3.70 Å in PM6:Y6 blends.[1] The equivalent interplanar spacing shows a marked increase for PM6:Y6:6Bx (20wt%) to 4.63 ± 0.08 Å. These results corroborate interpretation of the observed nanoscale heterogeneity with cross-linker content that influences the local morphology, a point that will be further discussed by solid-state NMR spectroscopy.

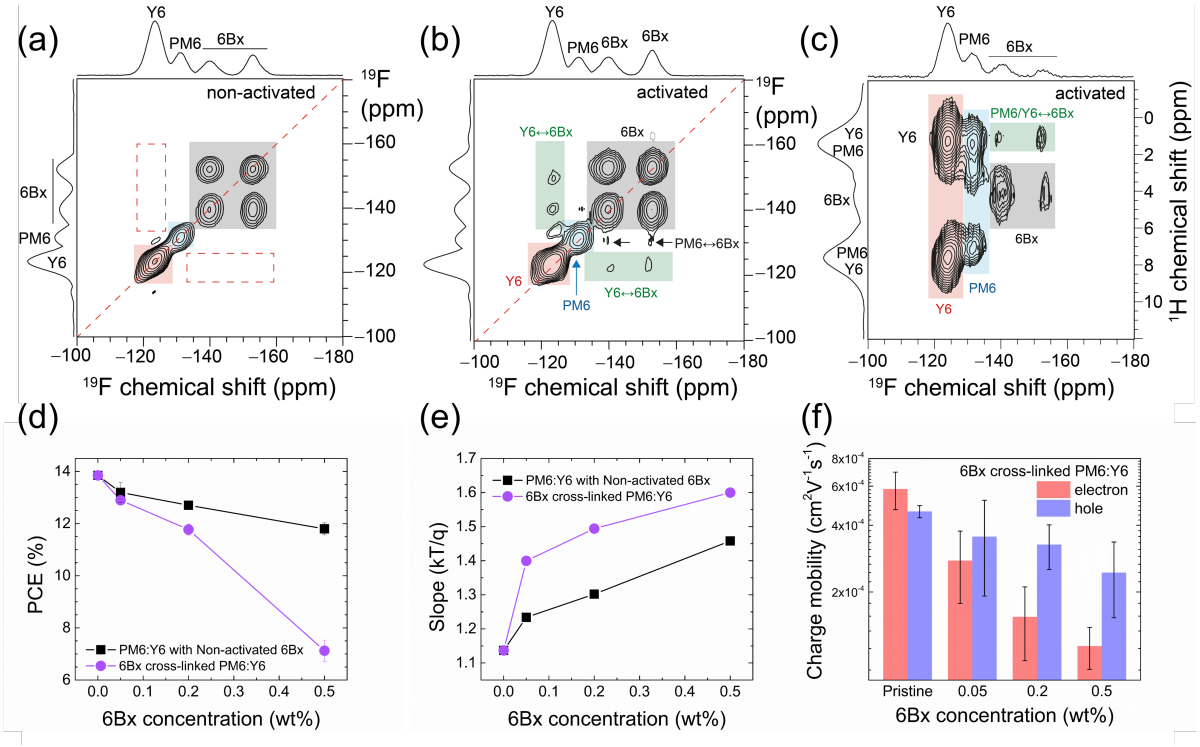

Figure 4. Solid-state 2D ^{19}F-^{19}F spin-diffusion (SD) NMR spectra of PM6:Y6 with 6Bx (a) before and (b) after UV photoactivation, acquired at 18.8 T with 1000 ms of SD mixing time. (c) 2D ^{19}F-^{1}H cross-polarization heteronuclear correlation (CP-HETCOR) NMR spectrum of the 6Bx cross-linked PM6:Y6 (after UV photoactivation), acquired at 20 T with 0.2 ms of CP contact time. (d) PCE values and (e) the slope of the V_{oc}-*ln(I)* plot for (black) the PM6:Y6 with non-activated 6Bx and (purple) the 6Bx cross-linked PM6:Y6 BHJ OPVs as a function of the 6Bx concentration. (f) SCLC charge carrier mobility of the PM6:Y6 blends and 6Bx cross-linked PM6:Y6 devices as a function of the 6Bx concentration.

Next, we investigated the bulk morphology of PM6:Y6 BHJ blends with 6Bx (20wt%) at a sub-nanometer resolution by solid-state nuclear magnetic resonance (ssNMR) and electron paramagnetic resonance (ssEPR) spectroscopy. A unique feature of these techniques is that they provide insights into the local structures of azide moieties from 6Bx and their interactions with the PM6 and Y6 molecules in heterogenous BHJ morphologies. Specifically, ssNMR has been increasingly applied to characterize polymeric semiconductors and their blends.[17, 77-79] Since the very low concentration of 6Bx (0.05wt%) is difficult to detect from SSNMR, we characterized the

BHJ blend with 20wt% 6Bx molecules. Among the nuclei probed in this study, ^{1}H and ^{13}C sites from PM6, Y6 and 6Bx produce overlapped spectra (**Figures S16** and **S17**), but ^{19}F sites gave rise to well-resolved patterns (**Figures S18-S20**). Identical ^{19}F chemical shifts for PM6 and Y6 in pristine and cross-linked BHJ morphology indicate that the acceptor domains are not significantly altered upon addition of 6Bx, consistently with the SED analysis. From the analysis of 1D ^{19}F NMR spectra alone, however, it remains unclear whether azide units are molecularly mixed and interact in the vicinity of PM6 and Y6 regions in the BHJ blend. In order to investigate the local structure, 2D ^{19}F-^{19}F and ^{19}F-^{1}H correlation experiments were conducted, in which chemical shifts and through-space proximities manifest as 2D peaks (**Figures S20-S21**). **Figure 4a** and **4b** compare 2D ^{19}F-^{19}F spin-diffusion (SD) NMR spectra of the PM6:Y6:6Bx BHJ before and after photoactivation, in which the on-diagonal peaks associated with PM6 (−131, red), Y6 (−125 ppm, blue) and 6Bx (−142 and −154 ppm, gray) moieties are well resolved. The off-diagonal peaks between 6Bx and Y6 s are exclusively detected in the photoactivated sample (**Figure 4b**, green boxes), but not for the non-activated sample (**Figure 4a**, red dashed boxes), confirming the through-space dipolar interactions between Y6 and 6Bx molecules. The off-diagonal peaks within the gray box are due to the close proximities of the different F atoms (*ortho* and *meta*) in the 6Bx molecules. Additionally, weak intensity peaks between the PM6 and 6Bx molecules (**Figure 4b**, black arrow) indicate that the 6Bx molecules interact less with the backbone moieties of PM6 or some traces of the 6Bx may be involved in PM6-6Bx-Y6 cross linking reactions. More evidently, the ^{19}F-^{1}H correlation NMR spectrum (**Figure 4c**) exhibits peaks corresponding to the through-space intermolecular H···F proximities in Y6, PM6 and 6Bx molecules as indicated by red, blue, and gray bands, respectively. For these samples, the line-cut 1D ^{1}H NMR spectra obtained from the 2D plot are presented in the SI (**Figure S21**). The most notable of all is that 2D peaks shown

in the green band (**Figure 4c**) indicate the close proximity between the PM6/Y6 sidechains and fluorinated aromatic groups (containing azide moieties) of the 6Bx molecules. This analysis aligns with the hypothesized C–H insertion reactions triggered by the photoactivation of azide moieties to generate a reactive singlet nitrene species.

The generated reactive species were further corroborated by continuous-wave (CW) EPR experiments and analysis (**Figure S22**). The 6Bx cross-linked PM6:Y6 BHJ exhibited EPR features with overlapping contribution from a narrow (4.5 Gauss) and a broader lineshape (15.8 Gauss) centered at a ***g*** value of 2.0048. The spin concentration in PM6:Y6:6Bx samples is 1.5×10^{14} spins/g, calculated using an external reference (weak pitch sample provided by the instrument manufacture). In contrast, the non-activated sample did not produce any EPR patterns. Raman spectroscopy analysis (**Figure S23**) of PM6, Y6, 6Bx compounds, and PM6:Y6:6Bx blends suggests a possible cross-linked site in Y6. For neat Y6, the peaks associated with the stretching vibrations (ν) of carbonyl (C=O) and nitrile (C≡N) groups were observed at ~1692 and 2212 cm^{-1} respectively, while the neat 6Bx shows peaks corresponding to the $\nu_{C=O}$ (~1740 cm^{-1}) and ν_{N3} (azide moieties, ~2130 cm^{-1}). The Raman spectra of a PM6:Y6:6Bx mixture acquired before and after photoactivation exhibited obvious changes in the vicinities of C=O and C≡N stretching modes of Y6 (**Figure S23b**), and increased intensities associated with C–H stretching modes upon photoactivation. The combined ssNMR, ssEPR and Raman spectroscopy analysis confirms the local structures and intermolecular proximities between 6Bx and Y6 molecules in the 6Bx cross-linked PM6:Y6 BHJ blend. These observations are further supported by analyzing miscibility parameters using contact angle measurements (SI, **Table S1**).

Following the detailed morphological and structural analysis of these materials, we then studied the impact of the 6Bx cross-linking on the photovoltaic properties of PM6:Y6 BHJ OPVs as a function of 6Bx concentration (0.05, 0.2, and 0.5 wt%). A slightly lower PCE of 13.92 ± 0.16% for PM6:Y6 OPVs (without 6Bx) is due to the batch dependence of the PM6 polymer discussed in our previous reports.[17, 76] The PCE values are significantly affected by the introduction of 6Bx at different concentrations (**Figure 4d**): 0.5 wt% of 6Bx in PM6:Y6 OPVs leads to 11.80 ± 0.23% and 7.12 ± 0.41% of PCE before and after photoactivation, respectively. In these devices, the reduced PCEs can be linked to trap-assisted recombination processes and charge carrier mobility. To understand the effect of 6Bx cross-linking on non-geminate recombination losses, light intensity (I) dependent open-circuit voltage (V_{oc}) analysis[80, 81] was carried out. The V_{oc}–ln(I) plot exhibits a linear relationship with a slope of kT/q when bimolecular recombination dominates, where k is the Boltzmann constant, T is absolute temperature, and q is the elementary charge. When bulk trap-assisted recombination dominates, the slope is larger than 1 kT/q. For PM6:Y6 BHJ OPVs with the 6Bx, the slope of the V_{oc}–ln(I) plot increases with higher 6Bx concentration (**Figure 4e**), which implies that addition of 6Bx into the PM6:Y6 BHJ causes additional bulk trap-assisted recombination. In order to explore how cross-linking affects electron and hole mobility, space-charge-limited current (SCLC) charge carrier mobilities of PM6:Y6 blends and PM6:Y6:6Bx were measured using electron- and hole-only diodes (see the SI for a detailed description). The electron and hole mobilities of these blends are presented in **Figure 4f**, and the values are summarized in **Table S2**. Both electron and hole mobilities decrease with higher 6Bx concentrations. 6Bx cross-linking influences the electron mobility much more than the hole mobility, which is consistent with the above-mentioned ssNMR results that suggested 6Bx molecules interact more closely with Y6 rather than PM6 in the PM6:Y6 BHJ. Thus, a relatively small concentration of 6Bx is preferred to

maintain reasonable OPV device performance, while enhancing device durability, as discussed below.

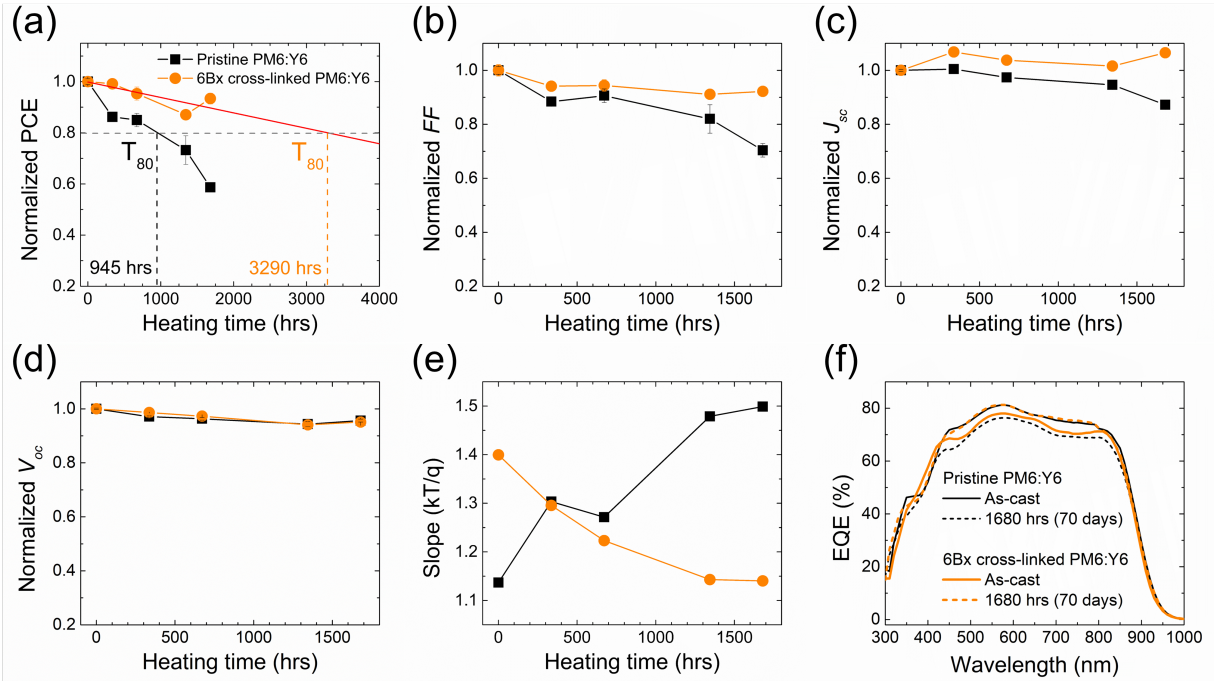

Figure 5. Normalized (a) PCE, (b) *FF*, (c) J_{sc}, (d) V_{oc}, and (e) the slope of the V_{oc}-*ln(I)* plot for (black) the pristine PM6:Y6 and (orange) 6Bx cross-linked PM6:Y6 BHJ OPVs as a function of thermal aging time at 85 °C. (f) EQE spectra of the pristine PM6:Y6 and 6Bx cross-linked PM6:Y6 BHJ OPVs before and after thermal aging at 85 °C for 1680 h.

For OPV durability tests, we used 0.05 wt% 6Bx cross-linked PM6:Y6 BHJ layers. Device parameters were recorded as a function of thermal aging time at 85 °C for up to 1680 h (70 days) in a nitrogen-filled glove box (see the experimental methods in the SI). The initial PCE (*i.e.* as-cast devices) of pristine PM6:Y6 BHJ and 6Bx cross-linked PM6:Y6 BHJ OPVs is 13.92 ± 0.16% and 12.53 ± 0.23%, respectively (**Table 2**). The normalized PV parameters of the pristine and cross-linked devices are shown in **Figure 5**, and the T_{80} (time lapsed to reach a PCE value at 80% of the initial value) was estimated (**Figure 5a**). It is evident that the T_{80} of the 6Bx cross-linked

PM6:Y6 BHJ OPVs even at a very low concentration is 3.48 times longer than that of the pristine devices under thermal aging. These results are further corroborated by the analysis of the fill factor (*FF*, **Figure 5b**), short circuit current (J_{sc}, **Figure 5c**) and V_{oc} (**Figure 5d**). Both V_{oc} and J_{sc} values of the cross-linked OPVs are well maintained after long-term thermal aging. On the other hand, the *FF* values are slightly reduced upon thermal aging. For the PM6:Y6 devices, the *FF* and J_{sc} decrease with thermal aging. The slope of the V_{oc}-ln*(I)* plot as a function of the aging time (**Figure 5e**) indicates that, in the early stage, the 6Bx cross-linked OPVs have a slightly larger slope value (1.39 *kT/q*) than that of the pristine OPVs (1.22 *kT/q*). However, it is surprising to observe that long-term thermal aging produces an opposite trend for the change in slope: the 6Bx cross-linked OPVs show reduced slope from 1.40 to 1.14 *kT/q*, whereas the slope of pristine OPVs increases from 1.14 to 1.50 *kT/q*. These results are further corroborated by the capacitance spectroscopy measurements and analysis (SI, **Figures S24-S26**). This observation agrees with the reduced *FF* and J_{sc} for pristine PM6:Y6 devices after thermal aging. The V_{oc}-ln*(I)* result indicates that trap-assisted recombination in 6Bx cross-linked OPVs is gradually mitigated, whereas the pristine OPVs show more severe trap-assisted recombination upon thermal aging, consistently with the previous work.[20, 82, 83] EQE spectra of the pristine PM6:Y6 and 6Bx cross-linked PM6:Y6 BHJ OPVs were measured before and after thermal aging, indicating that the 6Bx cross-linking contributed to improved EQE after aging (**Figure 5f**). This tendency is consistent with the J_{sc} results shown in **Figure 5c**.

Table 2. Photovoltaic parameters of the pristine PM6:Y6 and the 0.05 wt% 6Bx cross-linked PM6:Y6 BHJ OPVs before and after thermal aging at 85 °C for 1680 hours.

Pristine PM6:Y6	J_{sc} (mA/cm^2)	V_{oc} (V)	*FF*	PCE (%)
As-cast	25.75 ± 0.09	0.80 ± 0.002	0.68 ± 0.010	13.92 ± 0.16
Thermal Aging	22.46 ± 0.45	0.76 ± 0.004	0.48 ± 0.017	8.17 ± 0.26
0.05 wt% 6Bx cross-linked PM6:Y6				
As-cast	24.81 ± 0.15	0.78 ± 0.003	0.65 ± 0.014	12.53 ± 0.23
Thermal Aging	26.43 ± 0.43	0.74 ± 0.013	0.60 ± 0.010	11.70 ± 0.27

To recap, a facile and single-step molecular cross-linking strategy demonstrated in this study not only leads to suppressed molecular movement of the acceptor molecules, but also enhances thermal stability of BHJ OPVs. To understand the molecular origins that contribute to enhanced OPV stability, we characterized these materials at different length scales using electron diffraction and spectroscopy techniques. The 6Bx molecules efficiently cross-link the Y6 molecules in acceptor domains, as supported by an analysis of local structures at sub-nanometer resolution enabled by 2D ^{19}F-^{19}F and ^{19}F-^{1}H NMR spectroscopy techniques. Analysis of miscibility parameters using contact angle measurements support these results. These results are corroborated with device parameter analysis. These findings deepen our understanding of cross-linking strategies involving D and A molecules in the BHJ morphology, offering the potential to improve the lifetime of OPVs. This study utilized six-armed azide moiety to improve cross-linking densities, although higher loadings of cross-linker potentially dilute the active material and affects the optoelectronic properties through trap-assisted recombination. Improving morphological stability of NFAs using cross-linker additives avoids costly and intricate synthesis, making it particularly attractive. Therefore, photo-included cross-linking approaches are likely to find a promising future in OPVs research.

ASSOCIATED CONTENT

Supporting Information

Experimental methods, additional UV-vis absorption spectroscopy data, AFM and OM images, TGA thermogram, FTIR spectra, ssNMR spectra, EPR spectra, Raman spectra, summary of charge carrier mobility.

AUTHOR INFORMATION

Corresponding Authors

Thuc-Quyen Nguyen − *Center for Polymers and Organic Solids, Department of Chemistry and Biochemistry, University of California, Santa Barbara (UCSB), California 93106, United States; Email: quyen@chem.ucsb.edu*

G. N. Manjunatha Reddy − *University of Lille, CNRS, Centrale Lille Institut, Université d'Artois, UMR 8181, Unité de Catalyse et Chimie du Solide, Lille F-59000, France; E-mail: gnm.reddy@univ-lille.fr*

BongSoo Kim − *Department of Chemistry, Ulsan National Institute of Science and Technology (UNIST), Ulsan 44919, Republic of Korea; E-mail: bongsoo@unist.ac.kr*

Authors

Sangcheol Yoon − *Center for Polymers and Organic Solids, Department of Chemistry and Biochemistry, University of California, Santa Barbara (UCSB), California 93106, United States*

Braulio Reyes-Suárez − *University of Lille, CNRS, Centrale Lille Institut, Université d' Artois, UMR 8181, Unité de Catalyse et Chimie du Solide, Lille F-59000, France*

Sang T Pham – *Bragg Centre for Materials Research & School of Chemical and Process Engineering, University of Leeds, Woodhouse Lane, Leeds LS2 9JT, UK;*

Hervé Vezin − *University of Lille, CNRS UMR 8516 – LASIRE – Laboratoire de Spectroscopie pour les Interactions la Réactivité et l'Environnement Lille 59000, France*

Yeny A. Tobon − *University of Lille, CNRS UMR 8516 – LASIRE – Laboratoire de Spectroscopie pour les Interactions la Réactivité et l'Environnement Lille 59000, France*

Myeongjae Lee − *Department of Chemistry, Ulsan National Institute of Science and Technology (UNIST), Ulsan 44919, Republic of Korea*

Sam Mugiraneza − *Center for Polymers and Organic Solids, Department of Chemistry and Biochemistry, University of California, Santa Barbara (UCSB), California 93106, United States*

Brian Minki Kim − *Center for Polymers and Organic Solids, Department of Chemistry and Biochemistry, University of California, Santa Barbara (UCSB), California 93106, United States*

Mariane Yuka Tsubaki Oide − *Center for Polymers and Organic Solids, Department of Chemistry and Biochemistry, University of California, Santa Barbara (UCSB), California 93106, United States; Department of Metallurgical and Materials Engineering, University of São Paulo, São Paulo 05508-030, Brazil*

Seongju Yoo − *Department of Chemistry, Ulsan National Institute of Science and Technology (UNIST), Ulsan 44919, Republic of Korea*

Seunggu Lee − *Department of Physics and Research Institute of Basic Sciences, Kyung Hee University, Seoul 02447, Republic of Korea*

Shu Hui Wang − *Department of Metallurgical and Materials Engineering, University of São Paulo, São Paulo 05508-030, Brazil*

Sean M. Collins – *Bragg Centre for Materials Research & School of Chemical and Process Engineering, University of Leeds, Woodhouse Lane, Leeds LS2 9JT, UK; School of Chemistry, University of Leeds, Woodhouse Lane, Leeds LS2 9JT, UK*

Christopher M. Bates − *Department of Materials, Department of Chemistry and Biochemistry, Department of Chemical Engineering, University of California, Santa Barbara (UCSB), California 93106, United States*

Yongsup Park − *Department of Physics, Department of Information Display, Research Institute of Basic Sciences, Kyung Hee University, Seoul 02447, Republic of Korea*

Notes

The authors declare no competing financial interest.

ACKNOWLEDGMENTS

This work is supported by the US Office of Naval Research (Award No. N00014-21-1-2181). B. K was supported by the Samsung Research Funding and Incubation Center of Samsung Electronics (SRFC-MA1901-51). G. N. M. R. and H. V. gratefully acknowledges the support from EU H2020

research and innovation program under the Marie Skłodowska-Curie grant (No. 795091), and the support from the INFRANALYTICS FR-2054 CNRS France for conducting ssNMR and EPR measurements. S. H. W. and M. Y. T. O. were financially supported by the Coordenação de Aperfeiçoamento de Pessoal de Nível Superior – Brazil (CAPES) – Finance Code 001 and Conselho Nacional de Desenvolvimento Científico e Tecnológico - Brazil (CNPq) - Finance Code 141483/2019-9. Y. P and S. L. were supported by Korea Basic Science Institute (National research Facilities and Equipment Center) grant funded by the Ministry of Education (2021R1A6C101A437). The authors acknowledge funding support from the UK's Engineering and Physical Sciences Research Council (EPSRC, EP/V044907/1). We thank the Diamond Light Source, Rutherford Appleton Laboratory, UK, for access to the electron Physical Sciences Imaging Centre (ePSIC, MG34607). We thank Dr Mohsen Danaie and Dr Christopher Allen for support at ePSIC. The authors thank Dr. Patchareepond (Tam) Panoy, Dr. Hoang M. Luong, and Professor Craig Hawker for helpful discussions. C.M.B. thanks the Materials Research Science and Engineering Center (MRSEC) at UC Santa Barbara (NSF DMR-2308708, IRG-1) for funding.

REFERENCES

1. Yuan, J.; Zhang, Y.; Zhou, L.; Zhang, G.; Yip, H.-L.; Lau, T.-K.; Lu, X.; Zhu, C.; Peng, H.; Johnson, P. A.; Leclerc, M.; Cao, Y.; Ulanski, J.; Li, Y.; Zou, Y., Single-Junction Organic Solar Cell with over 15% Efficiency Using Fused-Ring Acceptor with Electron-Deficient Core. *Joule* **2019,** *3* (4), 1140-1151.
2. Schweda, B.; Reinfelds, M.; Hofstadler, P.; Trimmel, G.; Rath, T., Recent Progress in the Design of Fused-Ring Non-Fullerene Acceptors-Relations between Molecular Structure and Optical, Electronic, and Photovoltaic Properties. *ACS applied energy materials* **2021,** *4* (11), 11899-11981.
3. Kim, M.; Ryu, S. U.; Park, S. A.; Pu, Y. J.; Park, T., Designs and understanding of small molecule-based non-fullerene acceptors for realizing commercially viable organic photovoltaics. *Chemical science* **2021,** *12* (42), 14004-14023.
4. Li, S.; Li, C.-Z.; Shi, M.; Chen, H., New Phase for Organic Solar Cell Research: Emergence of Y-Series Electron Acceptors and Their Perspectives. *ACS Energy Letters* **2020,** *5* (5), 1554-1567.
5. Qin, F.; Li, G.; Liu, Y.; Cho, Y.; Pankow, R. M.; Zhang, D.; Feng, L.; Wang, Y.; Jeong, S.; Forti, G.; Zheng, D.; Yang, C.; Zhou, Y.; Marks, T. J.; Facchetti, A., Conjugated versus Nonconjugated Polymerized Small-Molecule Acceptors. Photovoltaic Response and Mechanical Properties. *ACS Energy Letters* **2023,** *8* (11), 4733-4745.
6. Lan, A.; Lv, Y.; Zhu, J.; Lu, H.; Do, H.; Chen, Z.-K.; Zhou, J.; Wang, H.; Chen, F.; Zhou, E., High-Performance Ternary Organic Solar Cells through Incorporation of a Series of A2-A1-D-A1-A2 Type Nonfullerene Acceptors with Different Terminal Groups. *ACS Energy Letters* **2022,** *7* (8), 2845-2855.

7. Kataria, M.; Chau, H. D.; Kwon, N. Y.; Park, S. H.; Cho, M. J.; Choi, D. H., Y-Series-Based Polymer Acceptors for High-Performance All-Polymer Solar Cells in Binary and Non-binary Systems. *ACS Energy Letters* **2022,** *7* (11), 3835-3854.

8. Chen, Z.; Zhu, J.; Yang, D.; Song, W.; Shi, J.; Ge, J.; Guo, Y.; Tong, X.; Chen, F.; Ge, Z., Isomerization strategy on a non-fullerene guest acceptor for stable organic solar cells with over 19% efficiency. *Energy & Environmental Science* **2023,** *16* (7), 3119-3127.

9. Liu, Z.; Zhang, M.; Zhang, L.; Jeong, S. Y.; Geng, S.; Woo, H. Y.; Zhang, J.; Zhang, F.; Ma, X., Over 19.1% efficiency for sequentially spin-coated polymer solar cells by employing ternary strategy. *Chemical Engineering Journal* **2023,** *471*, 144711.

10. Gan, Z.; Wang, L.; Cai, J.; Guo, C.; Chen, C.; Li, D.; Fu, Y.; Zhou, B.; Sun, Y.; Liu, C.; Zhou, J.; Liu, D.; Li, W.; Wang, T., Electrostatic force promoted intermolecular stacking of polymer donors toward 19.4% efficiency binary organic solar cells. *Nature communications* **2023,** *14* (1), 6297.

11. Lu, H.; Liu, W.; Ran, G.; Liang, Z.; Li, H.; Wei, N.; Wu, H.; Ma, Z.; Liu, Y.; Zhang, W.; Xu, X.; Bo, Z., High-Pressure Fabrication of Binary Organic Solar Cells with High Molecular Weight D18 Yields Record 19.65 % Efficiency. *Angewandte Chemie* **2023**, e202314420.

12. Ding, K.; Li, Y.; Forrest, S. R., Characterizing and Improving the Thermal Stability of Organic Photovoltaics Based on Halogen-Rich Non-Fullerene Acceptors. *ACS applied materials & interfaces* **2022,** *14* (4), 5692-5698.

13. Yang, Y.; Xiao, Y.; Xu, B.; Hou, J., Cross-Linkable Cathode Interlayer for Inverted Organic Solar Cells with Enhanced Efficiency and Stability. *Advanced Energy Materials* **2023**, *13*, 2301098.

14. Yin, Z.; Mei, S.; Gu, P.; Wang, H. Q.; Song, W., Efficient organic solar cells with superior stability based on PM6:BTP-eC9 blend and AZO/Al cathode. *iScience* **2021,** *24* (9), 103027.

15. Yao, J.; Qiu, B.; Zhang, Z. G.; Xue, L.; Wang, R.; Zhang, C.; Chen, S.; Zhou, Q.; Sun, C.; Yang, C.; Xiao, M.; Meng, L.; Li, Y., Cathode engineering with perylene-diimide interlayer enabling over 17% efficiency single-junction organic solar cells. *Nature communications* **2020,** *11* (1), 2726.

16. Jiang, Y.; Dong, X.; Sun, L.; Liu, T.; Qin, F.; Xie, C.; Jiang, P.; Hu, L.; Lu, X.; Zhou, X.; Meng, W.; Li, N.; Brabec, C. J.; Zhou, Y., An alcohol-dispersed conducting polymer complex for fully printable organic solar cells with improved stability. *Nature Energy* **2022,** *7* (4), 352-359.

17. Yoon, S.; Schopp, N.; Choi, D. G.; Wakidi, H.; Ding, K.; Ade, H.; Vezin, H.; Reddy, G. N. M.; Nguyen, T.-Q., Influences of Metal Electrodes on Stability of Non-Fullerene Acceptor-Based Organic Photovoltaics. *Advanced Functional Materials* **2024**, *34*, 2308618.

18. Lee, S.; Jin, J. S.; Moon, H.; Kim, J.-H.; Park, K.; Oh, J.; Ki, T.; Jang, S.-Y.; Kang, H.; Kim, H.; Lee, K., Long-Term Thermal Stability of Nonfullerene Organic Solar Cells via Facile Self-Assembled Interface Passivation. *ACS Energy Letters* **2023,** *8* (10), 3989-3998.

19. Ghasemi, M.; Hu, H.; Peng, Z.; Rech, J. J.; Angunawela, I.; Carpenter, J. H.; Stuard, S. J.; Wadsworth, A.; McCulloch, I.; You, W.; Ade, H., Delineation of Thermodynamic and Kinetic Factors that Control Stability in Non-fullerene Organic Solar Cells. *Joule* **2019,** *3* (5), 1328-1348.

20. Qin, Y.; Balar, N.; Peng, Z.; Gadisa, A.; Angunawela, I.; Bagui, A.; Kashani, S.; Hou, J.; Ade, H., The performance-stability conundrum of BTP-based organic solar cells. *Joule* **2021,** *5* (8), 2129-2147.

21. Ghasemi, M.; Balar, N.; Peng, Z.; Hu, H.; Qin, Y.; Kim, T.; Rech, J. J.; Bidwell, M.; Mask, W.; McCulloch, I.; You, W.; Amassian, A.; Risko, C.; O'Connor, B. T.; Ade, H., A molecular interaction-diffusion framework for predicting organic solar cell stability. *Nature materials* **2021,** *20* (4), 525-532.

22. Du, X.; Heumueller, T.; Gruber, W.; Classen, A.; Unruh, T.; Li, N.; Brabec, C. J., Efficient Polymer Solar Cells Based on Non-fullerene Acceptors with Potential Device Lifetime Approaching 10 Years. *Joule* **2019,** *3* (1), 215-226.

23. Wang, Y.; Luke, J.; Privitera, A.; Rolland, N.; Labanti, C.; Londi, G.; Lemaur, V.; Toolan, D. T. W.; Sneyd, A. J.; Jeong, S.; Qian, D.; Olivier, Y.; Sorace, L.; Kim, J.-S.; Beljonne, D.; Li, Z.; Gillett, A. J., The critical role of the donor polymer in the stability of high-performance non-fullerene acceptor organic solar cells. *Joule* **2023,** *7* (4), 810-829.

24. Clarke, A. J.; Luke, J.; Meitzner, R.; Wu, J.; Wang, Y.; Lee, H. K. H.; Speller, E. M.; Bristow, H.; Cha, H.; Newman, M. J.; Hooper, K.; Evans, A.; Gao, F.; Hoppe, H.; McCulloch, I.; Schubert, U. S.; Watson, T. M.; Durrant, J. R.; Tsoi, W. C.; Kim, J.-S.; Li, Z., Non-fullerene acceptor photostability and its impact on organic solar cell lifetime. *Cell Reports Physical Science* **2021,** *2* (7), 100498.

25. Du, X.; Heumueller, T.; Gruber, W.; Almora, O.; Classen, A.; Qu, J.; He, F.; Unruh, T.; Li, N.; Brabec, C. J., Unraveling the Microstructure-Related Device Stability for Polymer Solar Cells Based on Nonfullerene Small-Molecular Acceptors. *Advanced materials* **2020,** *32* (16), e1908305.

26. Zhao, Y.; Wu, Z.; Liu, X.; Zhong, Z.; Zhu, R.; Yu, J., Revealing the photo-degradation mechanism of PM6:Y6 based high-efficiency organic solar cells. *Journal of Materials Chemistry C* **2021,** *9* (39), 13972-13980.

27. Gasparini, N.; Paleti, S. H. K.; Bertrandie, J.; Cai, G.; Zhang, G.; Wadsworth, A.; Lu, X.; Yip, H.-L.; McCulloch, I.; Baran, D., Exploiting Ternary Blends for Improved Photostability in High-Efficiency Organic Solar Cells. *ACS Energy Letters* **2020,** *5* (5), 1371-1379.

28. Fan, B.; Gao, W.; Wang, Y.; Zhong, W.; Lin, F.; Li, W. J.; Huang, F.; Yu, K.-M.; Jen, A. K. Y., Formation of Vitrified Solid Solution Enables Simultaneously Efficient and Stable Organic Solar Cells. *ACS Energy Letters* **2021,** *6* (10), 3522-3529.

29. Skoplaki, E.; Boudouvis, A. G.; Palyvos, J. A., A simple correlation for the operating temperature of photovoltaic modules of arbitrary mounting. *Solar Energy Materials and Solar Cells* **2008,** *92* (11), 1393-1402.

30. Faiman, D., Assessing the outdoor operating temperature of photovoltaic modules. *Progress in Photovoltaics: Research and Applications* **2008,** *16* (4), 307-315.

31. Sun, C.; Lee, J.-W.; Lee, C.; Lee, D.; Cho, S.; Kwon, S.-K.; Kim, B. J.; Kim, Y.-H., Dimerized small-molecule acceptors enable efficient and stable organic solar cells. *Joule* **2023,** *7* (2), 416-430.

32. Tsai, C. H.; Li, F. N.; Liao, C. Y.; Su, Y. Y.; Tsai, K. W.; Hsiao, Y. T.; Chang, Y. M., Dimerized Small-Molecular Acceptor Enables the Organic Bulk-Heterojunction Layer with High Thermal Stability. *ACS applied materials & interfaces* **2023,** *15* (23), 27975-27983.

33. Lee, J.-W.; Sun, C.; Phan, T. N.-L.; Lee, D. C.; Tan, Z.; Jeon, H.; Cho, S.; Kwon, S.-K.; Kim, Y.-H.; Kim, B. J., Trimerized small-molecule acceptors enable high-performance organic solar cells with high open-circuit voltage and prolonged life-time. *Energy & Environmental Science* **2023**, *16*, 3339.

34. Sun, C.; Lee, J. W.; Tan, Z.; Phan, T. N. L.; Han, D.; Lee, H. G.; Lee, S.; Kwon, S. K.; Kim, B. J.; Kim, Y. H., Regiospecific Incorporation of Acetylene Linker in High-Electron

Mobility Dimerized Acceptors for Organic Solar Cells with High Efficiency (18.8%) and Long 1-Sun Lifetime (> 5000 h). *Advanced Energy Materials* **2023**, *13*, 2301283.

35. Bai, Y.; Zhang, Z.; Zhou, Q.; Geng, H.; Chen, Q.; Kim, S.; Zhang, R.; Zhang, C.; Chang, B.; Li, S.; Fu, H.; Xue, L.; Wang, H.; Li, W.; Chen, W.; Gao, M.; Ye, L.; Zhou, Y.; Ouyang, Y.; Zhang, C.; Gao, F.; Yang, C.; Li, Y.; Zhang, Z. G., Geometry design of tethered small-molecule acceptor enables highly stable and efficient polymer solar cells. *Nature communications* **2023,** *14* (1), 2926.
36. Fan, B.; Gao, W.; Zhang, R.; Kaminsky, W.; Lin, F. R.; Xia, X.; Fan, Q.; Li, Y.; An, Y.; Wu, Y.; Liu, M.; Lu, X.; Li, W. J.; Yip, H. L.; Gao, F.; Jen, A. K., Correlation of Local Isomerization Induced Lateral and Terminal Torsions with Performance and Stability of Organic Photovoltaics. *Journal of the American Chemical Society* **2023,** *145* (10), 5909-5919.
37. Fan, B.; Gao, W.; Wu, X.; Xia, X.; Wu, Y.; Lin, F. R.; Fan, Q.; Lu, X.; Li, W. J.; Ma, W.; Jen, A. K., Importance of structural hinderance in performance-stability equilibrium of organic photovoltaics. *Nature communications* **2022,** *13* (1), 5946.
38. Cho, Y.; Sun, Z.; Lee, K. M.; Zeng, G.; Jeong, S.; Yang, S.; Lee, J. E.; Lee, B.; Kang, S.-H.; Li, Y.; Li, Y.; Kwak, S. K.; Yang, C., CF3-Terminated Side Chain Enables Efficiencies Surpassing 18.2% and 16.1% in Small- and Large-Scale Manufacturing of Organic Solar Cells. *ACS Energy Letters* **2023,** *8* (1), 96-106.
39. Ma, Z.; Zhao, B.; Gao, H.; Gong, Y.; Yu, R.; Tan, Z. a., Recent advances of crosslinkable organic semiconductors in achieving solution-processed and stable optoelectronic devices. *Journal of Materials Chemistry A* **2022,** *10* (36), 18542-18576.

40. Wu, S. C.; Strover, L. T.; Yao, X.; Chen, X. Q.; Xiao, W. J.; Liu, L. N.; Wang, J.; Visoly-Fisher, I.; Katz, E. A.; Li, W. S., UV-Cross-linkable Donor-Acceptor Polymers Bearing a Photostable Conjugated Backbone for Efficient and Stable Organic Photovoltaics. *ACS applied materials & interfaces* **2018,** *10* (41), 35430-35440.

41. Kim, B. J.; Miyamoto, Y.; Ma, B.; Fréchet, J. M. J., Photocrosslinkable Polythiophenes for Efficient, Thermally Stable, Organic Photovoltaics. *Advanced Functional Materials* **2009,** *19* (14), 2273-2281.

42. Cheng, Y.-J.; Hsieh, C.-H.; Li, P.-J.; Hsu, C.-S., Morphological Stabilization by In Situ Polymerization of Fullerene Derivatives Leading to Efficient, Thermally Stable Organic Photovoltaics. *Advanced Functional Materials* **2011,** *21* (9), 1723-1732.

43. Derue, L.; Dautel, O.; Tournebize, A.; Drees, M.; Pan, H.; Berthumeyrie, S.; Pavageau, B.; Cloutet, E.; Chambon, S.; Hirsch, L.; Rivaton, A.; Hudhomme, P.; Facchetti, A.; Wantz, G., Thermal stabilisation of polymer-fullerene bulk heterojunction morphology for efficient photovoltaic solar cells. *Advanced materials* **2014,** *26* (33), 5831-8.

44. Yau, C. P.; Wang, S.; Treat, N. D.; Fei, Z.; Tremolet de Villers, B. J.; Chabinyc, M. L.; Heeney, M., Investigation of Radical and Cationic Cross-Linking in High-Efficiency, Low Band Gap Solar Cell Polymers. *Advanced Energy Materials* **2015,** *5* (5), 1401228.

45. Rumer, J. W.; Ashraf, R. S.; Eisenmenger, N. D.; Huang, Z.; Meager, I.; Nielsen, C. B.; Schroeder, B. C.; Chabinyc, M. L.; McCulloch, I., Dual Function Additives: A Small Molecule Crosslinker for Enhanced Efficiency and Stability in Organic Solar Cells. *Advanced Energy Materials* **2015,** *5* (9), 1401426.

46. Landerer, D.; Sprau, C.; Baumann, D.; Pingel, P.; Leonhard, T.; Zimmermann, D.; Chochos, C. L.; Krüger, H.; Janietz, S.; Colsmann, A., Thermal Stabilization of the Bulk-

Heterojunction Morphology in Polymer:Fullerene Solar Cells Using a Bisazide Cross-Linker. *Solar RRL* **2019,** *3* (2), 1800266.

47. Tu, S.; Lin, X.; Xiao, L.; Zhen, H.; Wang, W.; Ling, Q., Boosting the overall stability of organic solar cells by crosslinking vinyl-functionalized polymer derived from PM6. *Materials Chemistry Frontiers* **2022,** *6* (9), 1150-1160.

48. Chau, H. D.; Park, S. H.; Jung, S. H.; Park, J. Y.; Kang, M. J.; Harit, A. K.; Woo, H. Y.; Cho, M. J.; Choi, D. H., Rational strategy to enhance the thermal stability of solar cell performance using a photocrosslinkable conjugated polymer. *Journal of Materials Chemistry A* **2023,** *11* (16), 8719-8729.

49. Kwon, N. Y.; Park, S. H.; Kang, H.; Kim, Y. U.; Chau, H. D.; Harit, A. K.; Woo, H. Y.; Yoon, H. J.; Cho, M. J.; Choi, D. H., Improved Stability of All-Polymer Solar Cells Using Crosslinkable Donor and Acceptor Polymers Bearing Vinyl Moieties in the Side-Chains. *ACS Applied Materials & Interfaces* **2021,** *13* (14), 16754-16765.

50. Chen, A. X.; Hilgar, J. D.; Samoylov, A. A.; Pazhankave, S. S.; Bunch, J. A.; Choudhary, K.; Esparza, G. L.; Lim, A.; Luo, X.; Chen, H.; Runser, R.; McCulloch, I.; Mei, J.; Hoover, C.; Printz, A. D.; Romero, N. A.; Lipomi, D. J., Increasing the Strength, Hardness, and Survivability of Semiconducting Polymers by Crosslinking. *Advanced Materials Interfaces* **2023,** *10* (3), 2202053.

51. Ma, Z.; Dong, Y.; Su, Y.-J.; Yu, R.; Gao, H.; Gong, Y.; Lee, Z.-Y.; Yang, C.; Hsu, C.-S.; Tan, Z. a., Morphological Stabilization in Organic Solar Cells via a Fluorene-Based Crosslinker for Enhanced Efficiency and Thermal Stability. *ACS Applied Materials & Interfaces* **2022,** *14* (1), 1187-1194.

52. Ryu, K. Y.; Lee, J.; Jun, T.; Lee, D.; Kim, B.; Ryu, D. Y.; Kim, K., Immobilization of Conjugated Polymer Domains for Highly Stable Non-Fullerene-Based Organic Solar Cells. *ACS Applied Materials & Interfaces* **2022,** *14* (20), 23474-23486.

53. Wang, Z.; Zhang, D.; Xu, M.; Liu, J.; He, J.; Yang, L.; Li, Z.; Gao, Y.; Shao, M., Intrinsically Stretchable Organic Solar Cells with Simultaneously Improved Mechanical Robustness and Morphological Stability Enabled by a Universal Crosslinking Strategy. *Small* **2022,** *18* (26), e2201589.

54. Suzuki, R.; Ochiai, Y.; Nakano, K.; Miyasaka, M.; Tajima, K., Detrimental Effects of "Universal" Singlet Photocrosslinkers in Organic Photovoltaics. *ACS applied energy materials* **2023,** *6* (9), 4982-4988.

55. Lee, M.; Choi, B.-i.; Ahn, P.; Choi, Y. Y.; Heo, Y.; Kim, J.; Min, J. H.; Shin, T. J.; Kim, K.; Choi, H.; Kweon, H.; Ho, D. H.; Yoon, J. I.; Kim, H.; Lee, E.; Kim, D. H.; Kwak, K.; Kang, M. S.; Cho, J. H.; Kim, B., Low-Voltage Organic Transistors with Carrier Mobilities over 10 cm2V–2s–1 Using Six-Branched Organic Azide. *Chemistry of Materials* **2022,** *34* (23), 10409-10423.

56. Kahle, F.-J.; Saller, C.; Köhler, A.; Strohriegl, P., Crosslinked Semiconductor Polymers for Photovoltaic Applications. *Advanced Energy Materials* **2017,** *7* (16), 1700306.

57. Schnapp, K. A.; Poe, R.; Leyva, E.; Soundararajan, N.; Platz, M. S., Exploratory photochemistry of fluorinated aryl azides. Implications for the design of photoaffinity labeling reagents. *Bioconjugate Chemistry* **1993,** *4* (2), 172-177.

58. Marcinek, A.; Platz, M. S.; Chan, S. Y.; Floresca, R.; Rajagopalan, K.; Golinski, M.; Watt, D., Unusually long lifetimes of the singlet nitrenes derived from 4-azido-2,3,5,6-tetrafluorobenzamides. *The Journal of Physical Chemistry* **1994,** *98* (2), 412-419.

59. Poe, R.; Schnapp, K.; Young, M. J. T.; Grayzar, J.; Platz, M. S., Chemistry and kinetics of singlet pentafluorophenylnitrene. *Journal of the American Chemical Society* **1992,** *114* (13), 5054-5067.

60. Khong, S. H.; Sivaramakrishnan, S.; Png, R. Q.; Wong, L. Y.; Chia, P. J.; Chua, L. L.; Ho, P. K. H., General Photo-Patterning of Polyelectrolyte Thin Films via Efficient Ionic Bis(Fluorinated Phenyl Azide) Photo-Crosslinkers and their Post-Deposition Modification. *Advanced Functional Materials* **2007,** *17* (14), 2490-2499.

61. Teo, D. W. Y.; Jamal, Z.; Seah, Q.-J.; Png, R.-Q.; Chua, L.-L., General bis(fluorophenyl azide) photo-crosslinkers for conjugated and non-conjugated polyelectrolytes. *Journal of Materials Chemistry C* **2020,** *8* (1), 253-261.

62. Kim, M. J.; Lee, M.; Min, H.; Kim, S.; Yang, J.; Kweon, H.; Lee, W.; Kim, D. H.; Choi, J. H.; Ryu, D. Y.; Kang, M. S.; Kim, B.; Cho, J. H., Universal three-dimensional crosslinker for all-photopatterned electronics. *Nature communications* **2020,** *11* (1), 1520.

63. Lee, J.; Kim, J. W.; Park, S. A.; Son, S. Y.; Choi, K.; Lee, W.; Kim, M.; Kim, J. Y.; Park, T., Study of Burn-In Loss in Green Solvent-Processed Ternary Blended Organic Photovoltaics Derived from UV-Crosslinkable Semiconducting Polymers and Nonfullerene Acceptors. *Advanced Energy Materials* **2019,** *9* (34), 1901829.

64. Panzer, F.; Bassler, H.; Kohler, A., Temperature Induced Order-Disorder Transition in Solutions of Conjugated Polymers Probed by Optical Spectroscopy. *The journal of physical chemistry letters* **2017,** *8* (1), 114-125.

65. Kroh, D.; Eller, F.; Schötz, K.; Wedler, S.; Perdigón-Toro, L.; Freychet, G.; Wei, Q.; Dörr, M.; Jones, D.; Zou, Y.; Herzig, E. M.; Neher, D.; Köhler, A., Identifying the

Signatures of Intermolecular Interactions in Blends of PM6 with Y6 and N4 Using Absorption Spectroscopy. *Advanced Functional Materials* **2022,** *32* (44), 2205711.

66. Scharsich, C.; Fischer, F. S. U.; Wilma, K.; Hildner, R.; Ludwigs, S.; Köhler, A., Revealing structure formation in PCPDTBT by optical spectroscopy. *Journal of Polymer Science Part B: Polymer Physics* **2015,** *53* (20), 1416-1430.
67. Luo, Z.; Yang, Z.; Fei, Z.; Li, K., Effect of crosslinking rate on the glass transition temperature of polyimide cross-linked silica aerogels. *Journal of Polymer Research* **2020,** *27* (9), 255.
68. Huang, M.; Liu, Y.; Klier, J.; Schiffman, J. D., High-Performance, UV-Curable Cross-Linked Films via Grafting of Hydroxyethyl Methacrylate Methylene Malonate. *Industrial & Engineering Chemistry Research* **2020,** *59* (10), 4542-4548.
69. Bermejo, J. S.; Ugarte, C. M., Influence of Cross-Linking Density on the Glass Transition and Structure of Chemically Cross-Linked PVA: A Molecular Dynamics Study. *Macromolecular Theory and Simulations* **2009,** *18* (6), 317-327.
70. Root, S. E.; Alkhadra, M. A.; Rodriquez, D.; Printz, A. D.; Lipomi, D. J., Measuring the Glass Transition Temperature of Conjugated Polymer Films with Ultraviolet–Visible Spectroscopy. *Chemistry of Materials* **2017,** *29* (7), 2646-2654.
71. Li, S.; Zhang, R.; Zhang, M.; Yao, J.; Peng, Z.; Chen, Q.; Zhang, C.; Chang, B.; Bai, Y.; Fu, H.; Ouyang, Y.; Zhang, C.; Steele, J. A.; Alshahrani, T.; Roeffaers, M. B. J.; Solano, E.; Meng, L.; Gao, F.; Li, Y.; Zhang, Z. G., Tethered Small-Molecule Acceptors Simultaneously Enhance the Efficiency and Stability of Polymer Solar Cells. *Advanced materials* **2023,** *35* (2), e2206563.

72. Gutierrez-Fernandez, E.; Scaccabarozzi, A. D.; Basu, A.; Solano, E.; Anthopoulos, T. D.; Martin, J., Y6 Organic Thin-Film Transistors with Electron Mobilities of 2.4 cm(2) V(-1) s(-1) via Microstructural Tuning. *Advanced science* **2022,** *9* (1), e2104977.

73. Chen, K.; Wei, H.; Chen, P. A.; Liu, Y.; Guo, J.; Xia, J.; Xie, H.; Qiu, X.; Hu, Y., Band-like transport in non-fullerene acceptor semiconductor Y6. *Frontiers of optoelectronics* **2022,** *15* (1), 26.

74. Panova, O.; Ophus, C.; Takacs, C. J.; Bustillo, K. C.; Balhorn, L.; Salleo, A.; Balsara, N.; Minor, A. M., Diffraction imaging of nanocrystalline structures in organic semiconductor molecular thin films. *Nature Materials* **2019,** *18* (8), 860-865.

75. Sneyd, A. J.; Fukui, T.; Paleček, D.; Prodhan, S.; Wagner, I.; Zhang, Y.; Sung, J.; Collins, S. M.; Slater, T. J. A.; Andaji-Garmaroudi, Z.; MacFarlane, L. R.; Garcia-Hernandez, J. D.; Wang, L.; Whittell, G. R.; Hodgkiss, J. M.; Chen, K.; Beljonne, D.; Manners, I.; Friend, R. H.; Rao, A., Efficient energy transport in an organic semiconductor mediated by transient exciton delocalization. *Science Advances* **2021,** *7* (32), eabh4232.

76. Karki, A.; Vollbrecht, J.; Gillett, A. J.; Xiao, S. S.; Yang, Y.; Peng, Z.; Schopp, N.; Dixon, A. L.; Yoon, S.; Schrock, M.; Ade, H.; Reddy, G. N. M.; Friend, R. H.; Nguyen, T.-Q., The role of bulk and interfacial morphology in charge generation, recombination, and extraction in non-fullerene acceptor organic solar cells. *Energy & Environmental Science* **2020,** *13* (10), 3679-3692.

77. Seifrid, M.; Reddy, G. N. M.; Chmelka, B. F.; Bazan, G. C., Insight into the structures and dynamics of organic semiconductors through solid-state NMR spectroscopy. *Nature Reviews Materials* **2020,** *5* (12), 910-930.

78. Dixon, A. L.; Vezin, H.; Nguyen, T.-Q.; Reddy, G. N. M., Structural insights into Lewis acid- and F4TCNQ-doped conjugated polymers by solid-state magnetic resonance spectroscopy. *Materials Horizons* **2022,** *9* (3), 981-990.

79. Raval, P.; Dhennin, M.; Vezin, H.; Pawlak, T.; Roussel, P.; Nguyen, T.-Q.; Manjunatha Reddy, G. N., Understanding the p-doping of spiroOMeTAD by tris(pentafluorophenyl)borane. *Electrochimica Acta* **2022,** *424*, 140602.

80. Proctor, C. M.; Nguyen, T.-Q., Effect of leakage current and shunt resistance on the light intensity dependence of organic solar cells. *Applied Physics Letters* **2015,** *106* (8), 083301.

81. Cowan, S. R.; Roy, A.; Heeger, A. J., Recombination in polymer-fullerene bulk heterojunction solar cells. *Physical Review B* **2010,** *82* (24).

82. Wöpke, C.; Göhler, C.; Saladina, M.; Du, X.; Nian, L.; Greve, C.; Zhu, C.; Yallum, K. M.; Hofstetter, Y. J.; Becker-Koch, D.; Li, N.; Heumüller, T.; Milekhin, I.; Zahn, D. R. T.; Brabec, C. J.; Banerji, N.; Vaynzof, Y.; Herzig, E. M.; MacKenzie, R. C. I.; Deibel, C., Traps and transport resistance are the next frontiers for stable non-fullerene acceptor solar cells. *Nature Communications* **2022,** *13* (1), 3786.

83. Alam, S.; Aldosari, H.; Petoukhoff, C. E.; Váry, T.; Althobaiti, W.; Alqurashi, M.; Tang, H.; Khan, J. I.; Nádaždy, V.; Müller-Buschbaum, P.; Welch, G. C.; Laquai, F., Thermally-Induced Degradation in PM6:Y6-Based Bulk Heterojunction Organic Solar Cells. *Advanced Functional Materials* **2024,** *34* (6), 2308076.